

# Constraints on the Evolution of the Galaxy Stellar Mass Function I: Role of Star Formation, Mergers and Stellar Stripping

E. Contini,<sup>\*</sup> X. Kang,<sup>†</sup> A.D. Romeo, Q. Xia

*Purple Mountain Observatory, the Partner Group of MPI für Astronomie, 2 West Beijing Road, Nanjing 210008, China*

27 December 2018

## ABSTRACT

We study the connection between the observed star formation rate-stellar mass (SFR- $M_*$ ) relation and the evolution of the stellar mass function (SMF) by means of a Subhalo Abundance Matching technique coupled to merger trees extracted from a N-body simulation. Our approach, which considers both galaxy mergers and stellar stripping, is to force the model to match the observed SMF at redshift  $z > 2$ , and let it evolve down to the present time according to the observed (SFR- $M_*$ ) relation. In this study, we use two different sets of SMFs and two SFR- $M_*$  relations: a simple power law redshift-dependent and a relation with a mass-dependent slope and redshift-dependent. Our analysis shows that the evolution of the SMF is more consistent with a SFR- $M_*$  relation redshift-dependent and with a mass-dependent slope, in agreement with predictions from other models of galaxy evolution and recent observations. In order to fully describe the evolution of the SMF, both mergers and stellar stripping must be considered, and we find that both have almost equal effects on the evolution of SMF at the massive end. The high-mass end of the SMF obtained by considering stellar stripping is in good agreement with recent observational data from the Sloan Digital Sky Survey (SDSS). Up to  $\log M_* \sim 11.2$ , our prediction at  $z=0.1$  is close to Li & White (2009) data, but the high-mass end ( $\log M_* > 11.2$ ) is in better agreement with D’Souza et al. (2015) data.

**Key words:** clusters: general - galaxies: evolution - galaxy: formation.

## 1 INTRODUCTION

An important goal of galaxies formation and evolution modelling is to understand the buildup of the stellar matter content in the Universe. This is achievable when observations at different redshifts can help models in constraining fundamental statistics, such as the stellar mass function (SMF) and its evolution with time. On one hand, the SMF describes the galaxy stellar mass distribution that we can directly observe, and on the other hand, its evolution with time provides a natural test for studying the physical processes responsible for the growth of galaxies. Therefore, the SMF can be used to constrain cosmological models and the physical processes taking place during galaxy formation. Recently, the redshift evolution of the SMF has been measured by several wide surveys (e.g., Pérez-González et al. 2008; Drory et al. 2009;

Marchesini et al. 2009; Santini et al. 2012; Moustakas et al. 2013; Muzzin et al. 2013; Ilbert et al. 2013; Tomczak et al. 2014; Tomczak et al. 2016). The FourStar Galaxy Evolution Survey (ZFOURGE, Tomczak et al. 2014) is the latest example of a wide and deep near-infrared survey, with a mass completeness around  $\log M_* \simeq 9.0$  at redshift  $z \simeq 2$ .

Another important statistical property is the relation between the star formation rate (SFR) of galaxies versus their stellar mass (SFR- $M_*$  relation, also called “*main sequence relationship*” (MS)), which describes the rate of star formation for galaxies with given stellar mass. The SFR- $M_*$  relation, generally assumed to be a linear relation in a log-plane, has been intensely examined during the recent past (Daddi et al. 2007; Elbaz et al. 2007; Rodighiero et al. 2011; Whitaker et al. 2012 2014; Shivaei et al. 2015; Tasca et al. 2015; Tomczak et al. 2016). Overall these studies found an associated (due to observational uncertainties) and intrinsic scatter. While the scatter of this relation is found to remain tight at least up to  $z \sim 1.5$  (Salmi et al. 2012), its slope is reported to vary between 0.6 and 1,

<sup>\*</sup> Email: [contini@pmo.ac.cn](mailto:contini@pmo.ac.cn)

<sup>†</sup> Email: [kangxi@pmo.ac.cn](mailto:kangxi@pmo.ac.cn)

depending mainly on sample definitions and star formation indicators. According to several works, a linear relation between SFR and  $M_*$  gets bent towards of lower SFRs for higher stellar masses (e.g., Karim et al. 2011; Whitaker et al. 2014; Tomczak et al. 2016). Moreover, it has been established that the normalisation of the SFR- $M_*$  relation is redshift-dependent (Brinchmann et al. 2004; Elbaz et al. 2007; Daddi et al. 2007; Noeske et al. 2007; Renzini 2009; Peng 2010; Lee et al. 2015), while much more controversial appears the redshift evolution of its slope.

The SMF and SFR- $M_*$  relation are independent observables, and in principle it is possible to combine the observed SMF at high redshift with the SFR- $M_*$  relation to obtain subsequent stellar mass functions of galaxies. Such an approach has been followed by several authors (e.g., Conroy & Wechsler 2009; Leja et al. 2015; Tomczak et al. 2016) in order to shed light on the connection between the two observed statistics. In fact, all studies so far have found that the two observations are inconsistent with the observed evolution of the SMF (Leja et al. 2014). How to self-consistently describe the relationship between these two statistics is currently a hot issue in the study of galaxy evolution.

Leja et al. (2015) followed the aforementioned approach by connecting the observed star-forming sequence and the observed evolution of the SMF, between  $0.2 < z < 2.5$ . Interestingly, their study suggests that a single slope of the star-forming sequence smaller than 0.9 at all masses and redshifts would result in a higher number density of intermediate stellar mass galaxies, close to the knee of the SMF. To alleviate the discrepancy, they suggest a broken power law with a shallower slope at high masses and find that such a SFR- $M_*$  relation better agrees with the SMF evolution, although the inferred SMF is still offset by 0.3 dex from the observed one. The result of their study clearly shows that a mass-dependent slope of the SFR- $M_*$  relation is then needed to reconcile the observed evolution of the SMF with that inferred by connecting the SFR- $M_*$  relation with the observed SMF at high-redshift. According to their study, neither mergers nor hidden low-mass quiescent galaxies not detected are likely to be responsible for the mismatch.

Similar conclusions have been reached in a very recent study by Tomczak et al. (2016). These authors took advantage of the ZFOURGE survey to examine the slope of the SFR- $M_*$  relation. They find a redshift-dependent relation not consistent with a single power-law. The slope becomes shallower above a given turnover mass that ranges from  $10^{9.5} - 10^{10.8} M_\odot$ . They use the evolving SFR- $M_*$  relation with redshift to generate star-formation histories of galaxies. By integrating the set of star-formation histories with time, they obtain mass-growth histories to compare to the mass growth from the evolution of the stellar mass function of Tomczak et al. (2014). They find a reasonable agreement between the observed and inferred SMFs, but also room for a more detailed investigation. According to their conclusions, their study implies that either the star-formation rates measurements are overestimated, or the growth of the Tomczak et al. (2014) mass function is too slow, or both.

Here, and in a forthcoming paper (Contini et al. in prep.), we want to address this issue, following a similar method such as those described above. In this study, we adopt a relatively new approach. We use accurate merger

trees constructed from N-body simulations of Kang et al. (2012), and set up the stellar mass of galaxies by using an abundance matching technique in order to match the observed SMF at high redshift. Thus, our initial SMF matches perfectly with the observed data. Then, we use two different flavours of the observed SFR- $M_*$  relation, a single power-law and a mass-dependent slope, to assign SFRs to galaxies at any given lower redshift. We let galaxies grow according to their star-formation histories given by the SFR- $M_*$  relation as a function of redshift, and via mergers. This method is in spirit similar to Conroy & Wechsler (2009), but we proceed in the opposite direction, trying to reconcile the evolution of the SMF coupled to the observed SFR- $M_*$  relation, rather than guessing the latter from the former. Compared to previous studies, our novelty lies in two aspects: a) we take advantage of real merger trees from N-body simulations, which provide us the accretion histories of galaxies; b) we include stellar stripping in the model. Our main goals are:

- 1) understand the role of the SFR- $M_*$  relation (power-law or mass-dependent slope);
- 2) understand the role of stellar stripping and mergers in the evolution of the SMF.

The paper is structured as follows: in Section 2 we describe in detail our approach to address the issue and the method followed. In Section 3 we show our results, which will be fully discussed in Section 4. Finally, in Section 5 we give our conclusions.

## 2 METHOD

The simulation used in this paper is based on Kang et al. (2012). We refer the readers to that paper for more details, while here we introduce the main prescriptions. The simulation was performed using the Gadget-2 code (Springel 2005) with cosmological parameters adopted from the WMAP7 data release (Komatsu et al. 2011), namely:  $\Omega_\lambda = 0.73$ ,  $\Omega_m = 0.27$ ,  $\Omega_b = 0.044$ ,  $h = 0.7$  and  $\sigma_8 = 0.81$ . The simulation box is  $200 Mpc/h$  on each side using  $1024^3$  particles, each with mass  $5.64 \cdot 10^8 M_\odot h^{-1}$ . The merger trees are constructed by following the subhaloes resolved in FOF haloes at each snapshot (e.g., Kang et al. 2005) making use of the algorithm SUBFIND (Springel et al. 2001).

To populate dark matter haloes with galaxies we use the so-called Subhalo Abundance Matching (ShAM) technique. This method, originally proposed by Vale & Ostriker (2004), is now widely-used in numerical simulations to connect galaxies with dark matter structures (Vale & Ostriker 2006; Conroy et al. 2006; Behroozi et al. 2010; Moster et al. 2010; Guo et al. 2010; Hearin et al. 2013; Guo & White 2014; Yamamoto et al. 2015; Chaves-Montero et al. 2015). The fundamental assumption relies on a monotonic mapping between a given galaxy property, typically luminosity or stellar mass, and a given property of subhaloes such as maximum mass or maximum circular velocity of the subhalo during its history. One advantage of this method is that it is relatively easy to use, because it requires very few assumptions and avoids the explicit modelling of the physics of galaxy formation. Unfortunately, this entails a loss of a large amount of information, that is, indeed, the main handicap of the modelling.

For the purpose of our study we need to connect galaxies and haloes at different times. We start by forcing the algorithm to match the observed SMF (see Section 2.1 for more details concerning the SMFs chosen) at a given redshift. The algorithm makes use of the merger-trees described above and sorts galaxies and haloes in mass. Finally, it links them in a one-to-one relation. As time passes by, new haloes can form. We populate them with galaxies having stellar masses in accordance with the stellar mass-halo mass relation given by the abundance matching technique applied at that redshift. From the redshift of the match ( $z_{\text{match}}$ ) we let galaxies evolve according to their merger histories (given by the merger trees) and to their star formation histories. At each redshift we assign SFRs to galaxies by means of the SFR- $M_*$  relation observed at that redshift (see Section 2.1), down to  $z = 0$ . In order to consider also tidal interactions between satellite galaxies and the potential well of their hosts, we implement in the model a simple prescription for stellar stripping (see Section 2.2 for details).

## 2.1 Stellar Mass Functions and SFR- $M_*$ relations

We use two sets of observed stellar mass functions and two different SFR- $M_*$  relations, a single power-law and a mass-dependent slope relation. The first set of SMFs is taken from Fontana et al. (2006), who use data from the GOODS-MUSIC catalog, from  $0.4 < z < 4$ . This catalog contains 2931 Ks-selected galaxies with multi-wavelength coverage extending from the U-band to the Spitzer 8  $\mu\text{m}$  band, of which 27 per cent have spectroscopic redshifts and the remaining fraction have accurate photometric redshifts. For this sample they apply a standard fitting procedure to measure stellar masses, and compute the SMF up to  $z \simeq 4$ . These authors use a Salpeter (Salpeter 1955) Initial Mass Function (IMF), while our algorithm makes use of a Chabrier IMF (Chabrier 2003). Following Longhetti & Saracco (2009), we have corrected their masses in order to be consistent with a Chabrier IMF by means of the following relation:

$$M_{\text{Cha}}^*(z) = 0.55 \cdot M_{\text{Sal}}^*(z).$$

The second set of SMFs has been constructed by Tomczak et al. (2014), using observations from the FourStar Galaxy Evolution Survey (ZFOURGE). These data represent the deepest measurements to date of the galaxy SMF in the redshift range  $0.2 < z < 3$ . ZFOURGE is composed of three  $11' \times 11'$  pointings with coverage in the CDFS (Giacconi et al. 2002), COSMOS (Capak et al. 2007) and UKIDSS (Lawrence et al. 2007). The ZFOURGE fields also take advantage of HST imaging taken as part of the CANDELS survey (Grogin et al. 2011; Koekemoer et al. 2011) and from the NEWFIRM Medium-Band Survey (NMBS; Whitaker et al. 2011).

Both sets of data have been fit with a single-Schechter (Schechter 1976) function, defined as:

$$\frac{\Phi(M)dM}{\ln(10)} = \phi^* \left[ 10^{(M-M^*)(1+\alpha^*)} \right] \exp \left( -10^{(M-M^*)} \right) dM(1)$$

where  $M = \log(M/M_\odot)$ ,  $\alpha^*$  is the slope at the low-mass end,  $\phi^*$  is the normalization and  $M^*$  is the characteristic mass. For the set of SMFs by Fontana et al. the three pa-

**Table 1.** Best fit of the seven free parameters in the set of equations 2. Note that  $M_0^*$  has been corrected for the different IMF. The original value in Fontana et al. is  $M_0^* = 11.16$ .

$M_0^*$	10.90
$M_1^*$	$+0.17 \pm 0.05$
$M_2^*$	$-0.07 \pm 0.01$
$\alpha_0^*$	-1.18
$\alpha_1^*$	$-0.082 \pm 0.033$
$\phi_0^*$	0.0035
$\phi_1^*$	$-2.20 \pm 0.18$

**Table 2.** Redshift, logarithm of the normalisation, slope at the low-mass end and logarithm of the characteristic mass for the set of SMFs by Tomczak et al..

Redshift	$\log(\phi^*)$	$\alpha^*$	$\log(M^*)$
0.3	$-2.96 \pm 0.10$	$-1.35 \pm 0.04$	$11.05 \pm 0.10$
0.6	$-2.93 \pm 0.07$	$-1.35 \pm 0.04$	$11.00 \pm 0.06$
0.8	$-3.17 \pm 0.11$	$-1.38 \pm 0.04$	$11.16 \pm 0.12$
1.1	$-3.19 \pm 0.11$	$-1.33 \pm 0.05$	$11.09 \pm 0.10$
1.3	$-3.11 \pm 0.08$	$-1.29 \pm 0.05$	$10.88 \pm 0.05$
1.8	$-3.28 \pm 0.08$	$-1.33 \pm 0.05$	$11.03 \pm 0.05$
2.2	$-3.59 \pm 0.14$	$-1.43 \pm 0.08$	$11.13 \pm 0.13$

rameters  $\alpha^*$ ,  $\phi^*$  and  $M^*$  evolve with redshift according to the following set of parameterisations:

$$\phi^*(z) = \phi_0^* \cdot (1+z)^{\phi_1^*}$$

$$\alpha^*(z) = \alpha_0^* + \alpha_1^* \cdot z \quad (2)$$

$$M^*(z) = M_0^* + M_1^* \cdot z + M_2^* \cdot z^2$$

where  $\phi_0^*$ ,  $\phi_1^*$ ,  $\alpha_0^*$ ,  $\alpha_1^*$ ,  $M_0^*$ ,  $M_1^*$  and  $M_2^*$  are free parameters which values are reported in Table 1. In Table 2 we report the values of the three parameters of the fits at different redshifts for Tomczak et al.'s set.

In order to account for star formation we use two SFR- $M_*$  relations: 1) a single power-law with normalisation redshift-dependent, and 2) a parameterised relation with a mass-dependent slope. The single power-law relation reads as follow:

$$\text{SFR}[M_\odot/\text{yr}] = 2.78 \cdot M_{*,10}^{0.9} \cdot (1+z)^{1.8}, \quad (3)$$

where  $M_{*,10}$  is the stellar mass in unit of  $10^{10} M_\odot$ . Equation 3 is a good representation of the SFR- $M_*$  relations suggested by Daddi et al. (2007) at  $z \sim 2$ , and Elbaz et al. (2007) at  $z \sim 1$ . For the relation with a mass-dependent slope we have chosen the parameterisation suggested by Tomczak et al. (2016) (see also Lee et al. 2015):

$$\log(\text{SFR}[M_\odot/\text{yr}]) = s_0 - \log \left[ 1 + \left( \frac{M_*}{M_0} \right)^\gamma \right], \quad (4)$$

where  $s_0$  and  $M_0$  are in units of  $\log(M_\odot/\text{yr})$  and  $M_\odot$  respectively. Equation 4, as explained by Tomczak et al. (2016), behaves as a normal power-law with slope  $\gamma$  at low masses, and asymptotically approaches a peak value  $s_0$  above a characteristic stellar mass  $M_0$ . Using data from the same survey used in Tomczak et al. (2014), these authors find that such a parameterisation works well even if quiescent galaxies are

considered. For this reason, we parameterise  $s_0$  and  $M_0$  with the same second-order polynomials valid for all galaxies:

$$\begin{aligned} s_0 &= 0.195 + 1.157z - 0.143z^2 \\ \log(M_0) &= 9.244 + 0.753z - 0.090z^2 \\ \gamma &= -1.118 \end{aligned} \quad (5)$$

Equation 4 and the set of equations 5 describe the evolution with time of the SFR- $M_*$  relation with a mass-dependent slope. Considering the fact that galaxies with the same mass but in different environments have different star formation rates, we assume that:

- central galaxies have 100 per cent of the star formation rate given by Eqs 3 and 4;
- satellite galaxies associated with a dark matter subhalo have 50 per cent of the star formation rate given by Eqs 3 and 4;
- satellite galaxies not embedded in a dark matter subhalo (sometime called as orphan galaxies) have 10 per cent of the star formation rate given by Eqs 3 and 4.

However, our results are not significantly affected by our assumptions, since the SMF is dominated by central galaxies over almost all the stellar mass range.

## 2.2 Stellar Stripping

Stellar stripping is an important process that takes place during galaxy formation and evolution. It has been shown by several authors (e.g. Purcell et al. 2007; Contini et al. 2014) that most of the diffuse light around galaxies forms through this channel. As highlighted in Section 1, no study that used a similar approach as ours considered the effect of stellar stripping on the evolution of the SMF, especially its role at redshift  $z < 1$ , when the bulk of the diffuse light starts to form (Murante et al. 2007; Contini et al. 2014). We model stellar stripping in a very simple fashion, assuming that the stellar mass lost due to disruption events and stripping can be parameterised by an exponential law such as:

$$M_{lost}^{z=z_i} = M_{*(s_1, s_2)}^{z=z_i} \cdot \exp\left(\frac{-\eta(M_{halo})(t_{infall} - t_i)}{\tau_{s1, s2}}\right), \quad (6)$$

where  $t_{infall}$  is the time when the galaxy last entered a cluster (i.e., became a satellite),  $t_i$  the cosmic time at  $z = z_i$ , and  $\tau_{s1, s2}$  two normalisations set to 30 Gyr and 15 Gyr, respectively, for satellites associated with a distinct dark matter substructure ( $s_1$ ), and orphan galaxies ( $s_2$ ). We set an higher normalisation for satellites  $s_1$  in order to consider the effect of dark matter in shielding the galaxy from tidal forces.  $\eta(M_{halo})$  is the stripping efficiency, chosen to be a function of the main halo mass ( $M_{200}^1$ ) in which satellites reside in order to consider the different strength of stellar stripping in haloes of different mass. We report in Table 3 the values of  $\eta$  for different halo mass ranges. This values have been chosen in order to reproduce as much as possible the observed abundance of satellites in groups and clusters (see Appendix A) by Yang et al. (2009).

<sup>1</sup>  $M_{200}$  is the mass within the virial radius  $R_{200}$ , defined as the radius that encloses a mean density of 200 times the critical density of the Universe at the redshift of interest.

**Table 3.** Stripping efficiency  $\eta$  (second line) as a function of the halo mass  $M_{200}$  in unit of  $M_\odot/h$  (first line).

$< 10^{13}$	$[1-5] \cdot 10^{13}$	$[5-10] \cdot 10^{13}$	$[1-5] \cdot 10^{14}$	$[5-10] \cdot 10^{14}$	$> 10^{15}$
1	0.8	0.5	0.3	0.2	0.1

In addition to stellar stripping, we consider another channel for the formation of the diffuse light, i.e. the so called "merger channel" (see e.g., Murante et al. 2007; Contini et al. 2014), to consider also those stars that might end up in the diffuse light getting unbound through relaxation processes that happen during galaxy-galaxy merging. We simply assume that when two galaxies merge, 30 per cent of the satellite stellar mass gets unbound and goes to the diffuse component.

## 3 RESULTS

In this section we show our model predictions compared with observed data, the two sets of SMFs presented in Section 2.1. For the sake of simplicity, we define:

- Model A: Fontana+06 SMFs coupled to the SFR- $M_*$  relation given by Equation 3;
- Model B: Tomczak+16 SMFs coupled to the SFR- $M_*$  relation given by Equation 3;
- Model C: Fontana+06 SMFs coupled to the SFR- $M_*$  relation given by Equation 4 and parameterisations given by the set of equations 5;
- Model D: Tomczak+16 SMFs coupled to the SFR- $M_*$  relation given by Equation 4 and parameterisations given by the set of equations 5.

Unless otherwise specified, all models will take into account galaxies mergers and stellar stripping (see Section 2.2).

### 3.1 Role of the SFR- $M_*$ relation

In Section 1 we pointed out that the role of the SFR- $M_*$  relation in shaping the evolution of the SMF is still under debate, especially the shape of such relation itself. A simple power-law (e.g., Daddi et al. 2007; Elbaz et al. 2007) might lead to predictions quantitatively different from those obtained by coupling the SMF at high- $z$  to a SFR- $M_*$  relation with a mass-dependent slope (e.g., Lee et al. 2015; Tomczak et al. 2016). Here we want to address this issue by looking at the evolution of the SMF as predicted by the four models described above.

In Figure 1 we plot the evolution of the SMF since  $z = 2.1$  as predicted by Model A, and compare our results with the observed evolution of the SMF by Fontana et al.. Stars represent our model data, while the solid and dashed lines represent Fontana et al. and our model data fits, respectively. We start at  $z_{match} = 2.6$  and since by construction our model prediction perfectly matches the observed SMF at  $z = 2.6$ , we do not show this redshift. As time passes by, our Model A over-predicts the high-mass end of the SMF and becomes unrealistic at  $z = 0.5$ . At this time, the SMF looks more like a power-law than a Schechter

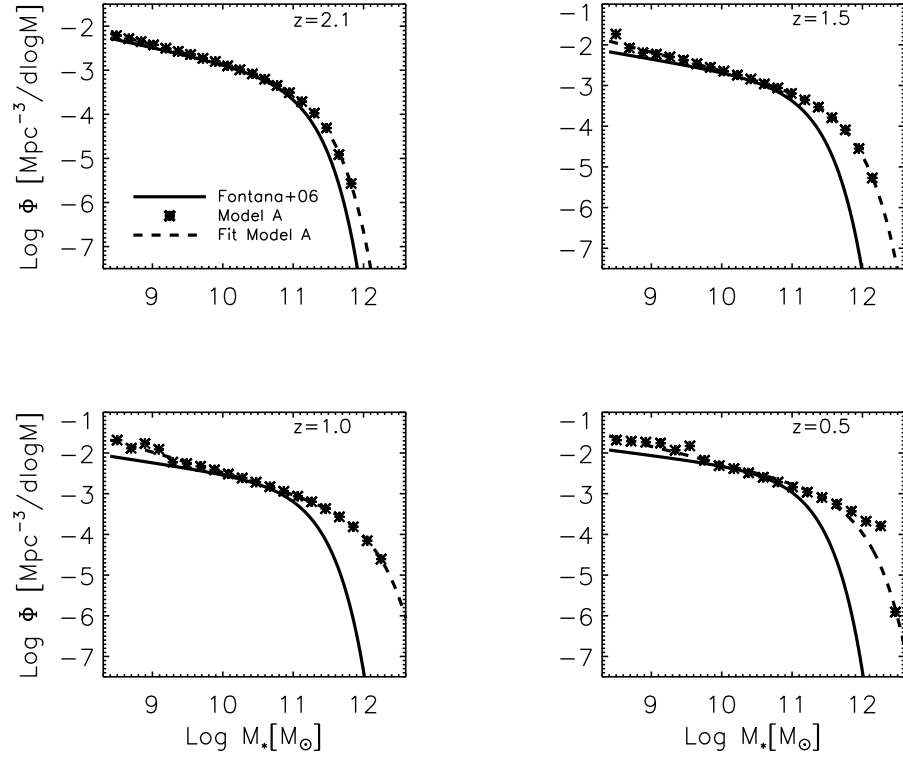


**Figure 1.** Evolution of the SMF from  $z = 2.1$  down to  $z = 0.5$  predicted by our Model A. Here we assume an initial SMF by Fontana+06 at  $z = 2.6$  and coupled to a SFR- $M_*$  relation with a single slope. Stars represent model data, the solid lines represent Fontana+06 fit and dashed lines the fits done on our model predictions.

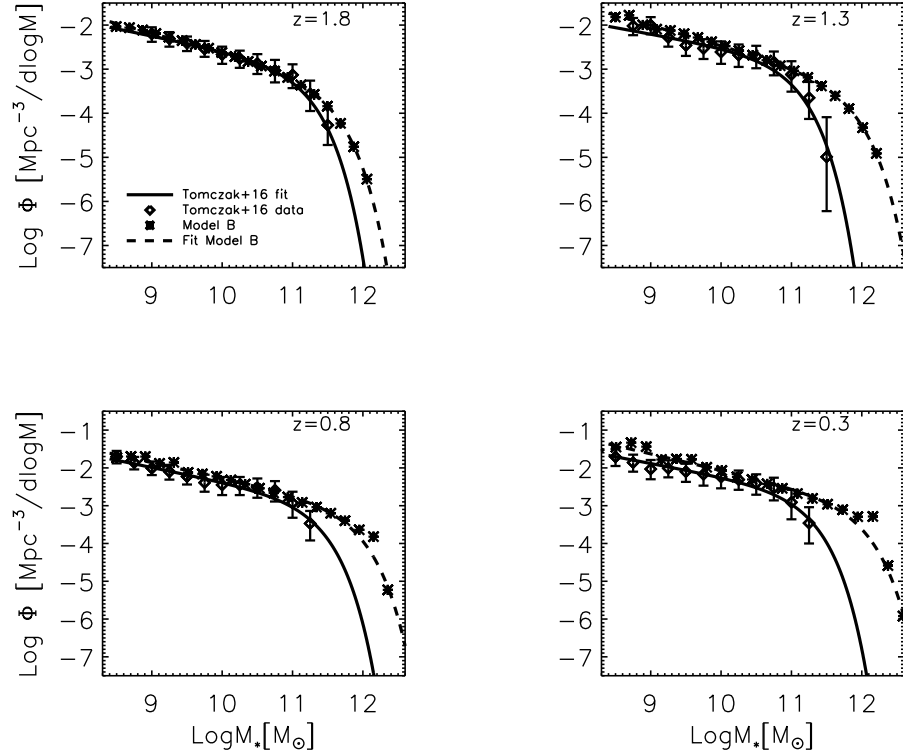


**Figure 2.** Evolution of the SMF from  $z = 1.8$  down to  $z \sim 0.3$  predicted by our Model B. Here we assume an initial SMF by Tomczak+16 at  $z = 2.2$  and coupled to a SFR- $M_*$  relation with a single slope. Stars and diamonds represent model and Tomczak+16 data, respectively, while the solid and dashed lines represent Tomczak+16 and our model prediction fits, respectively.

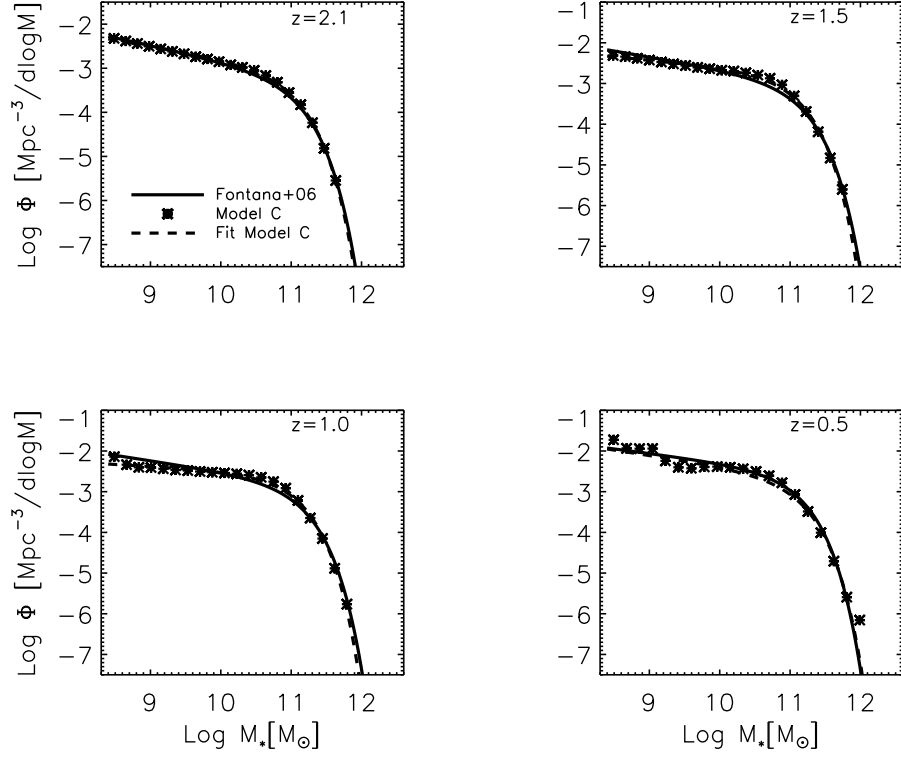


**Figure 3.** Evolution of the SMF from  $z = 2.1$  down to  $z = 0.5$  predicted by our Model C. Here we assume an initial SMF by Fontana+06 at  $z = 2.6$  and coupled to a SFR- $M_*$  relation with a mass-dependent slope. Stars represent model data, the solid lines represent Fontana+06 fit and dashed lines the fits done on our model predictions.

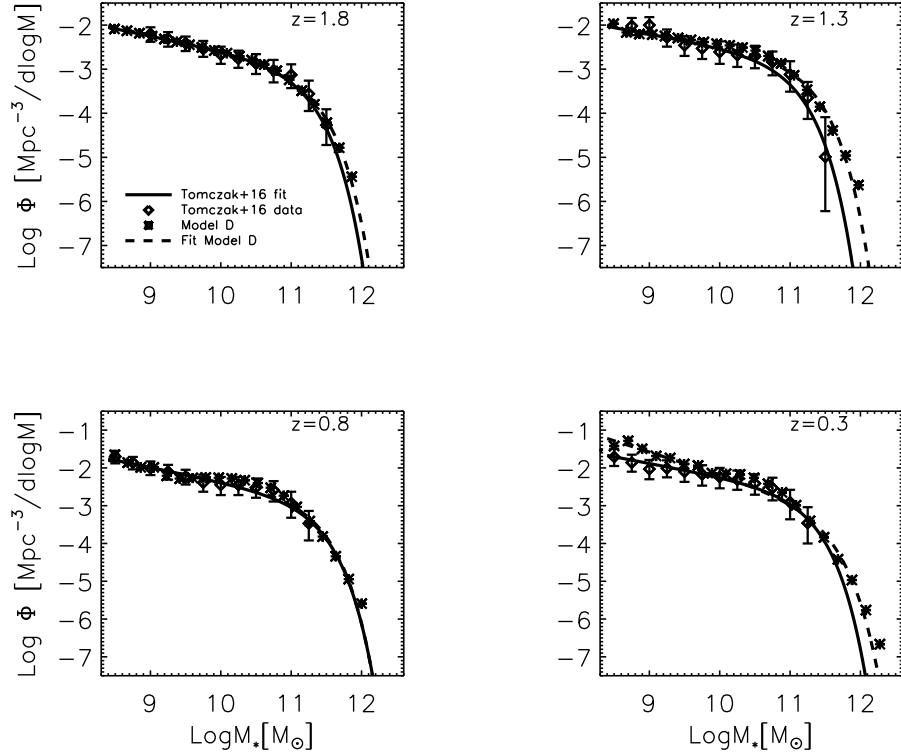


**Figure 4.** Evolution of the SMF from  $z = 1.8$  down to  $z \sim 0.3$  predicted by our Model D. Here we assume an initial SMF by Tomczak+16 at  $z = 2.2$  and coupled to a SFR- $M_*$  relation with a mass-dependent slope. Stars and diamonds represent model and Tomczak+16 data, respectively, while the solid and dashed lines represent Tomczak+16 and our model prediction fits, respectively.

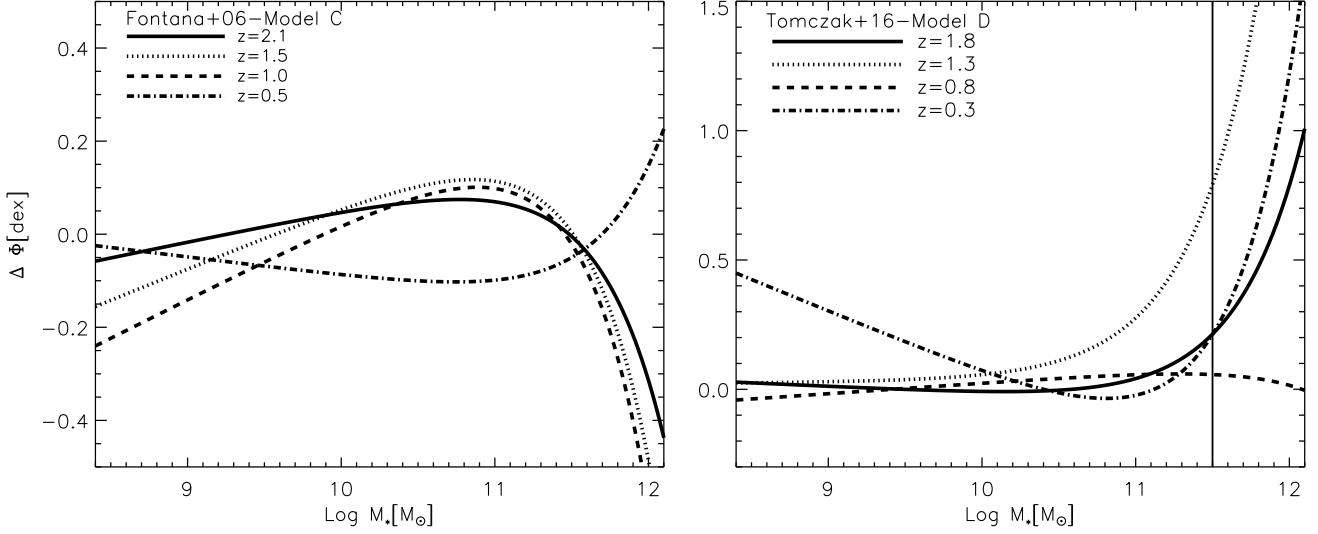


**Figure 5.** Left panel: residuals between the SMF predicted by our Model C and the observed one, at different redshift (different line styles as shown in the legend). Right panel: the same as the left panel, but for Model D. The solid vertical line in the right panel indicates the maximum stellar mass bin in Tomczak et al. data.

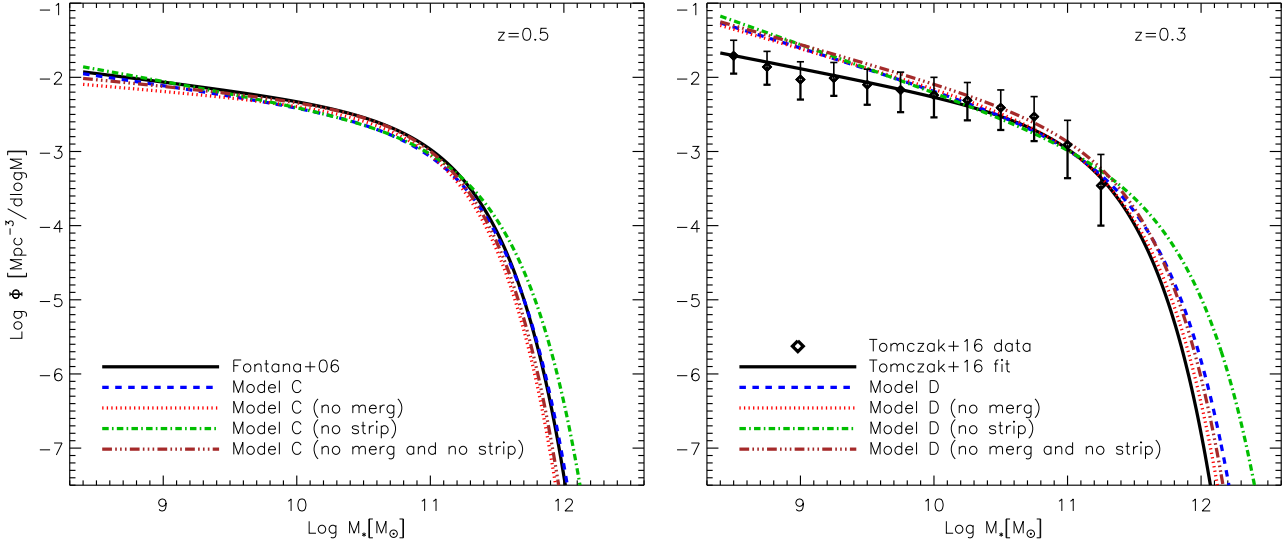


**Figure 6.** Left panel: predictions of the SMF at  $z = 0.5$  by different flavours of Model C (different line styles as shown in the legend), compared with the observed SMF. Right panel: the same as the left panel but for Model D, that is compared with the observed SMF at  $z \sim 0.3$ .

function. Hence, Model A highly over-predicts the number of massive galaxies since  $z = 1.5$ .

Figure 2 shows the evolution of the SMF since  $z = 1.8$  (and down to  $z \sim 0.3$ ) as predicted by Model B, and compare our results with the observed evolution of the SMF by Tomczak et al. (note that we do not show the panel corresponding to  $z = z_{\text{match}}$ , being  $z_{\text{match}} = 2.2$ ). Stars and diamonds represent model and Tomczak+16 data, respectively, while the solid and dashed lines represent Tomczak+16 and our model prediction fits, respectively. Over almost all the mass range shown by the observed data points, they agree fairly well with our predictions at all redshifts. Nevertheless, Model B shows the same problem as Model A, i.e. the number of massive galaxies is excessively over-predicted since

$z = 1.3$ . For both Model A and B we tried to switch off mergers in order not to let massive galaxies grow too much, but even in this case predictions do not get significantly closer to observed data (plot not shown). For these two models, the bulk of the growth of massive galaxies is due to their intense star formation history.

In Figure 3 we plot the evolution of the SMF as predicted by Model C, and similarly to Figure 1, we compare our results with the observed evolution of the SMF by Fontana et al. (line styles and symbols have the same meaning as in Figure 1). This model works reasonably well down to  $z = 0.5$ . It matches the high-mass end of the observed SMF at any redshift and shows small residuals in the low/intermediate stellar mass range. By comparing the evo-

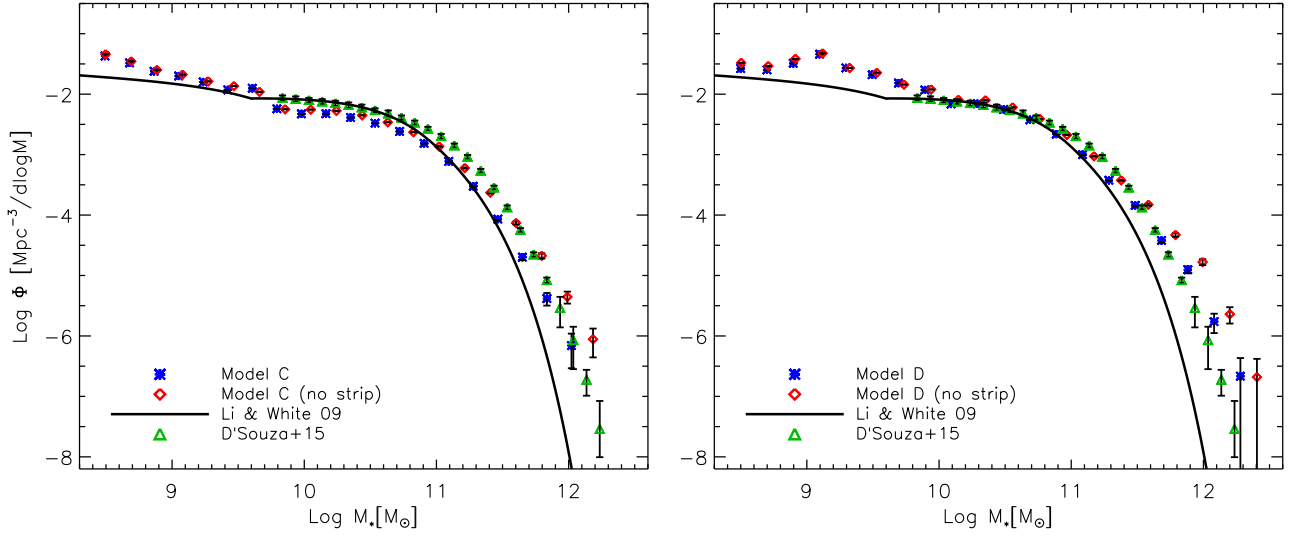


**Figure 7.** Left panel: predictions of the SMF at  $z \sim 0.1$  of our Model C with and without stellar stripping (stars and diamonds, respectively), compared with the observed SMF by Li & White 2009 (solid line) and D’Souza et al. 2015 (triangles). Right panel: the same as the left panel but for Model D.

lution of the SMF predicted by Model A (Figure 1) and the one predicted by Model C (Figure 3), i.e. the same set of observed SMFs, but a  $\text{SFR}-M_*$  relation with a single slope (Model A) versus a mass-dependent slope (Model C), a non-linear  $\text{SFR}-M_*$  relation is supported by our results.

Similarly to Figure 2, we show in Figure 4 the evolution of the SMF since  $z = 1.8$  (and down to  $z \sim 0.3$ ) as predicted by Model D, and compare our results with the observed evolution of the SMF by Tomczak et al. (line styles and symbols have the same meaning as in Figure 2). Also in this case the high-mass end is better reproduced by the model at all redshifts, and our predictions fairly reproduce observations down to redshift  $z = 0.3$ . Overall, Model D confirms that a mass-dependent slope of the  $\text{SFR}-M_*$  relation, rather than a single slope, is more consistent with the evolution of the SMF.

Having the idea that Model C and Model D provide an evolution of the SMF more in line with the observed one, we want to quantify in Figure 5 the deviation of the models from the observed SMF as a function of redshift, for Model C (left panel) and Model D (right panel). We plot the residuals in dex, i.e. the difference between the logarithm of the observed number density and the logarithm of the predicted number density, as a function of stellar mass and at different redshifts (as shown in the legend). In the left panel we can see that residuals are a function of stellar mass and tend to increase with decreasing redshift (with the exception of  $z = 0.5$ ). The left panel shows that Model D has the same trend shown by Model C, but with larger (in modulus) residuals in the high-mass end and lower in the intermediate/low-mass range, with respect to Model C (with the exception of the closest redshift to us).

### 3.2 Role of Mergers and Stellar Stripping

As explained in Section 1, most of the previous studies did not consider the role of mergers and stellar stripping in the evolution of the SMF. With our approach it is relatively

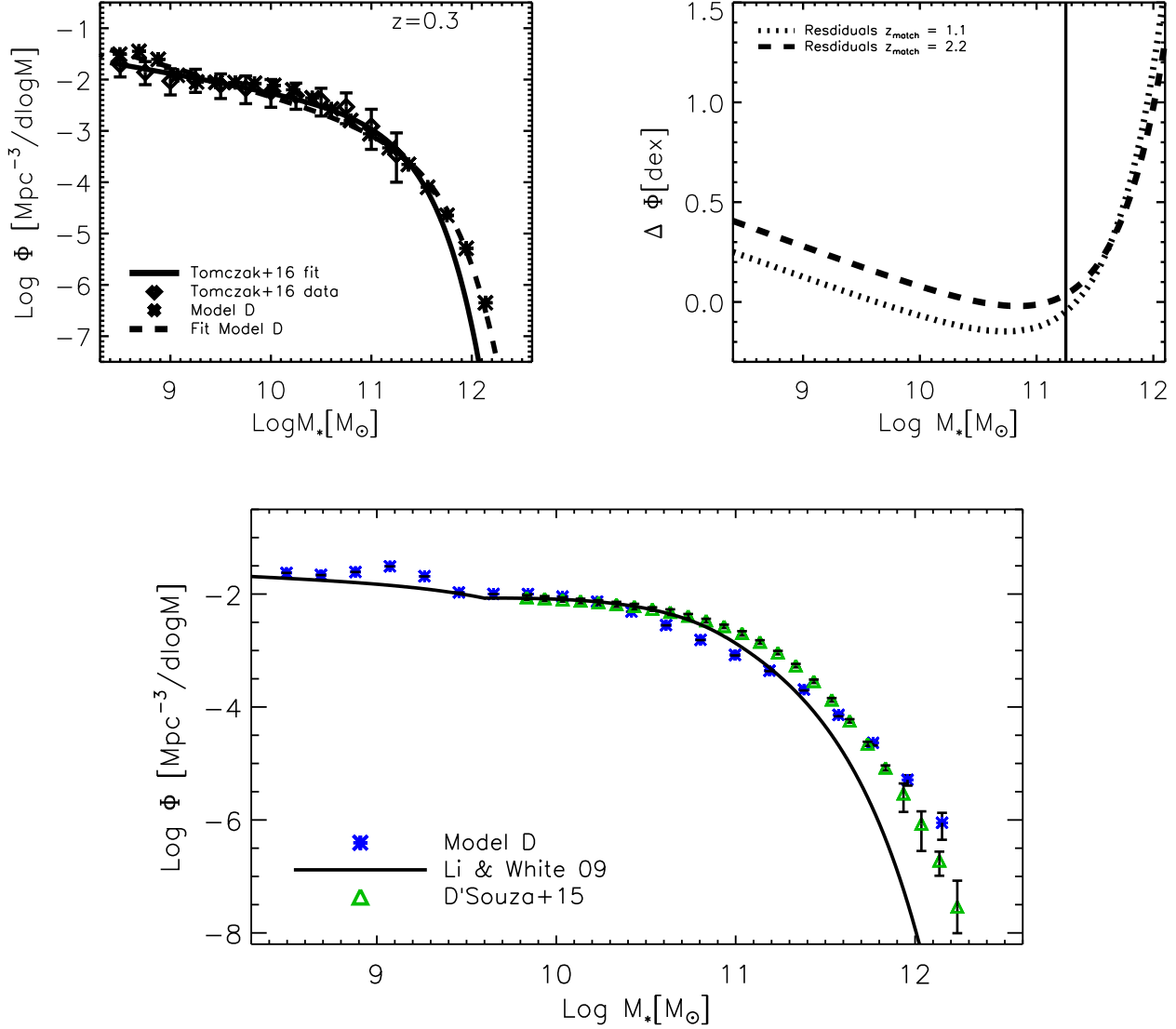
straightforward to isolate their contribution, just by switching on/off the prescriptions that account for them. The aim of this section is to prove that their role is not negligible, in particular that of stellar stripping.

Figure 6 shows the SMF at  $z = 0.5$  as predicted by Model C (left panel), and the SMF at  $z \sim 0.3$  as predicted by Model D (right panel). The figure also shows Model C/D when mergers are switched off (dotted lines), with no stellar stripping (dash-dotted lines), and when both mergers and stellar stripping are switched off (dash-long-dotted lines). Both panels show that if stripping is switched off, the high-mass end of the SMF is over-predicted. This is easily understandable because satellite galaxies do not grow too much, being subject to mass loss. What appears to be very interesting is the roles of mergers and stellar stripping altogether. In fact, dashed lines (full model) and dash-long-dotted lines (no mergers and no stripping) lie very close to each other, meaning that the two processes have opposite effects: mergers increase the mass of central galaxies (dash-dotted lines), while stellar stripping reduces the mass of satellite galaxies. This means that stellar stripping tend to let the SMF move towards the left and mergers towards the right<sup>2</sup>. Since they do not have exactly the same effect, quantitatively speaking a full model predicts higher number densities than a model with no stripping and no mergers, in the high-mass end.

It is worth noting that the intrinsic differences among models are significant only in the high-mass end, where the number density is lower and the merging/stellar stripping histories of single galaxies might make the difference. In the rest of the stellar mass range, from the low-mass end to the knee of the SMF, models have similar trends and the

<sup>2</sup> The SMF should move also towards lower number densities because of the smaller number of satellite galaxies. The plot does not show it since the SMF is dominated by central galaxies, especially in the low-mass end, where the number of satellites is supposed to decrease.





**Figure 8.** Top-left panel: SMFs at  $z \simeq 0.3$ . Here we assume an initial SMF by Tomczak+16 coupled to a SFR- $M_*$  relation with a mass-dependent slope (Model D), with  $z_{\text{match}} = 1.1$ . Stars and diamonds represent model and Tomczak+16 data, respectively, while the solid and dashed lines represent Tomczak+16 and our model prediction fits, respectively. Top-right panel: residuals between the SMF predicted by our Model D and the observed one at  $z \simeq 0.3$ , in case of  $z_{\text{match}} = 1.1$  (dotted line) and  $z_{\text{match}} = 2.2$  (dashed line). The solid vertical line indicates the maximum stellar mass bin in Tomczak et al. data at  $z \simeq 0.3$ . Bottom panel: SMF at  $z = 0.1$  as predicted by Model D and compared with the observed SMF by Li & White 2009 (solid line) and D’Souza et al. 2015 (triangles). Here  $z_{\text{match}} = 1.1$ .

observed scatter (see the right panel) is not sufficient to rule-out one (or more) of them.

### 3.3 Stellar Mass Function at low redshift

The lowest redshifts provided by the two sets of SMFs we have chosen are  $z = 0.5$  (Fontana et al.) and  $z = 0.3$  (Tomczak et al.). Nevertheless, if observations are consistent to each other, it is possible to let the SMF evolve down to the present time and compare the models predictions with the observed SMF from other surveys. One important point still under debate is the slope of the high-mass end of the SMF, that appears to be shallower than thought earlier. If this

is true, this translates in a higher number density of very massive galaxies.

Recently, D’Souza et al. (2015) compute the SMF at very low redshift for a sample of half a million galaxies from the Sloan Digital Sky Survey (SDSS) in the stellar mass range  $9.5 < \log(M_* [M_\odot h^{-2}]) < 12.0$ . As the authors point out, systematic differences in the estimation of the stellar mass of a galaxy can be due to a different choice of the IMF (for which there are, however, well constrained corrections), to the stellar mass-to-light ratio ( $M/L$ ), and to different estimations of the galaxy total flux. The key point of their work is the latter. Therefore, for the sample of galaxies used by Li & White (2009), they derive flux corrections to the model magnitudes by stacking together mosaics of similar

galaxies in bins of stellar mass and concentration, and re-derive the galaxy stellar mass function at redshift  $z = 0.1$ . They find that the flux corrections result in a higher massive end of the SMF and make the slope shallower than that found by Li & White 2009, but steeper than that estimated by Bernardi et al. (2013).

In Figure 7 we plot our models predictions at redshift  $z \sim 0.1$  for Model C (left panel) and Model D (right panel), with (stars) and without (diamonds) stellar stripping, and compare our results with the SMF computed by both Li & White (2009) (solid line) and D’Souza et al. (2015) (triangles). As we highlighted above, if stellar stripping is switched off it would result in a higher massive end, but too high if compared with the observed one, for either models, C and D. A model in which stellar stripping is switched on, instead, agrees fairly well with the observed SMF by D’Souza et al. (2015) in the intermediate stellar mass range (as a model with no stripping does), and lies closer to data than a model with no stripping up to the very massive end. It must be noted that the best prediction is given by Model D, while Model C under-predicts the number density in the intermediate stellar mass range. Therefore, according to these results, our models predictions, especially Model D, support an higher massive end, more in agreement with the observed high-mass end by D’Souza et al. (2015) than that by Li & White (2009) or by Bernardi et al. (2013). In principle, a model with no stellar stripping would be closer to the SMF by Bernardi et al. (2013) in the high mass end, being it higher than that found by D’Souza et al. (2015) (see Figure 7 of D’Souza et al.). Nevertheless, such a model cannot account for the abundance of satellite galaxies in haloes of different mass (see Figure A1 in Appendix A) that we have used to calibrate the stripping efficiency in our model of stellar stripping.

Problems arise in the low-mass end, where both models (C and D) over-predict the abundance of dwarf galaxies. This problem is more serious for Model D, for which the number density of galaxies with mass  $\log M_* < 10$  is over-predicted by up to a factor 0.5 dex (at  $\log M_* \sim 9.1$ ). We will come back on this issue in the next section.

## 4 DISCUSSION

In order for the  $SFR-M_*$  relation to be consistent with the observed evolution of the SMF, it would be important to consider all the uncertainties in measuring both the stellar mass of galaxies and their star formation rate. This point has been discussed by Leja et al. (2015), and somewhat considered by Tomczak et al. (2016). Given all the systematic uncertainties, it is possible, however, to discriminate between a  $SFR-M_*$  relation with a single power-law shape, and one with a mass-dependent slope. This is one of the main goals of this paper.

In Figures 1 and 2 we have shown that a single power-law shape cannot describe the evolution of the SMF, since for both sets of SMFs chosen this would bring to highly over-predict the high-mass end, giving to the SMF an unrealistic shape at low redshift. Nevertheless, these figures show that, especially with the set of SMFs by Tomczak et al. (2016), the slope of the  $SFR-M_*$  relation (0.9) for low-mass galaxies seems to be acceptable, since the low-mass end of the SMF is

reproduced at least down to  $z \sim 0.8$ . Likely, a slightly lower normalisation would be better because predictions lie lightly above observations at those redshifts and mass ranges (this is clearly shown in the case of our Model B, when the set of SMFs by Tomczak et al. is coupled to a single power-law). The actual problem does not concern the choice of the slope of the  $SFR-M_*$  relation itself, rather its whole shape and evolution with redshift.

To shed light on this issue, we have coupled the observed SMF to a  $SFR-M_*$  relation with a mass-dependent slope (Model C/D). Figures 3 and 4 show that such a relation gives much better predictions. First, the overall shape of the predicted SMF is comparable with the observed one, and second, the high-mass end at every redshift is better reproduced. Despite that, it is not enough to make the  $SFR-M_*$  relation and the observed evolution of the SMF be consistent one another. This has been shown in Figure 5, where the residuals between the observed and predicted SMFs increase with decreasing redshift, although we consider galaxy mergers and stellar stripping. Tomczak et al, who find a similar mismatch at all redshifts, argue that this disagreement implies that either the SFRs are overestimated and/or the observed growth of the Tomczak et al. (2014) SMF is too slow. Similar arguments have been discussed by other authors. Weinmann et al. (2012) show that, in order to reconcile the  $SFR-M_*$  relation with the growth of the SMF at  $z < 1$ , either the slope of this relation is greater than 0.9, or a high rate of destruction by mergers must be invoked. We have shown in Figure 6 that mergers cannot have such a relevant role, and the match substantially improves when stellar stripping is considered.

Similarly to Tomczak et al., we believe that the discrepancies are mainly due to errors in stellar mass and SFRs estimates. The formers make the observed SMF not 100 per cent reliable, in particular at high-redshift, and the latter will collect additional scatter around the SMF during its evolution. The observed SMF at high- $z$  is not 100 per cent accurate, and this is testified by the fact that different observed SMFs do not match each other, as those we have chosen. Tomczak et al. find similar residuals, in particular in the low/intermediate stellar mass range. They use the same evolving  $SFR-M_*$  relation with redshift (Equation 4) to generate star-formation histories of galaxies, and integrate the set of star-formation histories with time. They then obtain mass-growth histories to compare with the mass growth from the evolution of the stellar mass function of Tomczak et al. (2014). This method is in spirit similar to that used in this paper, but they let the SMF evolve for a limited time (see their Figure 10). Moreover, their method does not account for galaxy mergers and stripping. By comparing the observed and inferred SMFs, they conclude that a reasonable match would require between 25-65 per cent of the excess galaxies to merge with a more massive galaxy per Gyr. This definitely exceeds current estimates of galaxy merger rates (e.g. Lotz et al. 2011; Williams et al. 2011; Leja et al. 2015). In Tomczak et al., they assign SFR (according to  $SFR-M_*$  relation) to all galaxies, but in principle satellite galaxies should have lower SFR. In their model they do not classify galaxies into centrals and satellites. This could lead to too much growth in stellar mass in their model.

In our study we let the SMF evolve with time starting from high-redshift and down to low-redshift, according

to the same evolution with redshift given by the SFR- $M_*$  relation used by Tomczak et al. In the case of Model D, that is the set of SMFs by Tomczak et al. 2014 coupled to the SFR- $M_*$  relation given by Equation 4, we start at  $z_{\text{match}} \simeq 2.2$  and let the SMF grow down to  $z \simeq 0.3$ . As said above, during this time systematic uncertainties both in the stellar mass and SFR estimates can propagate, thus increasing the mismatch between the observed and inferred SMFs. If we restrict the evolution of the SMF by lowering  $z_{\text{match}}$ , where both the stellar mass and SFR measurements should be more reliable, we then expect a better match, which translates in smaller residuals. We test this argument in Figure 8, where  $z_{\text{match}}$  has been set to 1.1, and the SMF evolves down to  $z \simeq 0.1$ , for Model D. As we can see, the SMF at  $z = 0.3$  predicted by the model (top-left panel) is more in agreement with the observed one, being residuals around 0.2 dex smaller (top-right panel). This implies that if we let the SMF evolve for a shorter time, errors on the measurements of the SFRs have a shorter time for propagating, resulting in smaller residuals. From low stellar masses to  $\log M_* = 11.25$ , which corresponds to the maximum stellar mass bin in Tomczak et al. data at  $z \simeq 0.3$  (vertical solid line in the top-right panel of Figure 8), and where both fits are more accurate, residuals decrease from a maximum of 0.4 dex (dashed line, low-mass) to 0.25 dex (dotted line, low-mass), while the minimum is close to 0 in both cases (at  $\log M_* \sim 10.8$ ). It is worth noting also that we obtain comparable (with respect to Tomczak et al.) residuals if  $z_{\text{match}} = 2.2$ , and smaller if  $z_{\text{match}}$  is lower, because we are taking into account most of the processes that can influence galaxy growth, such as mergers and stellar stripping (not considered by Tomczak et al.).

In the bottom panel of Figure 8 we plot the SMF at  $z = 0.1$  as predicted by Model D (with  $z_{\text{match}} = 1.1$ ), and compared with the observed ones (by Li & White 2009 and D’Souza et al. 2015), as done in Figure 7. In Section 3.3 we highlighted that Model D over-predicts the low-mass end of the SMF at  $z = 0.1$  by a non-negligible factor (around 0.5 dex at  $\log M_* \sim 9.1$ ). This panel shows that, when the match is done at a lower redshift, the low-mass end is more in agreement with observed data. Overall, Figure 8 demonstrates that our modelling is very sensitive to the shape of the SMF and in particular the slope of the low-mass end, not only to the SFR- $M_*$  relation. The slope of the low-mass end constrains the number of low-mass galaxies that have to grow. A steep slope of the SMF at high-redshift would bring to over-predict the number density of low/intermediate stellar mass galaxies, and a shallow slope would act in the other direction.

## 5 CONCLUSIONS

We have analysed the stellar mass growth of galaxies from  $z > 2$  taking advantage of the Subhalo Abundance Matching method. We have linked the observed SFR- $M_*$  relation to the observed SMF at high-redshift to study its evolution with time. In this paper, two sets of SMFs and two different SFR- $M_*$  relations have been chosen: the set of SMFs by Fontana et al. 2006 (GOODS-MUSIC catalog), and the set of SMFs by Tomczak et al. 2014 (ZFOURGE catalog). Both sets of SMFs have been coupled to: (1) a SFR- $M_*$  relation

with a single power-law shape, and a redshift-dependent normalisation (Equation 3), and: (2) SFR- $M_*$  relation redshift-dependent and with a mass-dependent slope (Equations 4 and 5). From our analysis we conclude that:

- The evolution of the stellar mass function is much more consistent with a SFR- $M_*$  relation redshift-dependent and with a mass-dependent slope, rather than a simple single power-law. If coupled to a SFR- $M_*$  with a single power-law, the SMF would not have a Schechter shape at low-redshift. Moreover, the number density of high stellar mass galaxies ( $\log M_* > 11.2 - 11.3$ ) would be greatly over-predicted at any redshift. This is in agreement with predictions of other models of galaxy evolution, semi-analytic, hydrodynamical, and abundance-matching models (e.g. Weinmann et al. 2012; Leja et al. 2015), and supported by observations (e.g. Whitaker et al. 2014; Tomczak et al. 2016).
- Galaxy mergers and stellar stripping are physical processes that must be taken into account in order to fully analyse the evolution of the SMF. We have shown that both mergers and stripping are important in shaping the massive end of the SMF.
- The observed SMF at high- $z$  is not 100 per cent accurate. We have tested two different sets of SMFs coupled to the same SFR- $M_*$  relation and same modelling for mergers and stellar stripping. They result in different evolutions down to low-redshift.
- The observed high-mass end at very low redshift is not yet accurate. We have shown that our models predictions favour an higher massive end than that estimated by Li & White 2009, more in agreement with recent results by D’Souza et al. 2015.
- The inferred evolution of the stellar mass function is sensitive to the shape of the observed SMF at  $z = z_{\text{match}}$ . Moreover, during the evolution of the SMF systematic uncertainties both in the stellar mass and SFR estimates can propagate, thus increasing the mismatch between the observed and inferred SMFs. We have shown that, if the inferred SMF starts to evolve when stellar mass and SFR measurements are more reliable, and uncertainties have less time to propagate, the match at low-redshift is characterised by rather smaller residuals.

Although the match between the observed and inferred SMFs has improved with respect to previous studies, given by the fact that mergers are taken into account by using accurate merger trees and stellar stripping is modelled, there is still something missing. It might be due to one or more of the aforementioned problematics, or to any other process that we are not yet considering. In a forthcoming paper, we will re-address this issue by means of a slightly different approach. We use the set of SMFs by Tomczak et al. 2014 coupled to the observed SFR- $M_*$  with a mass-dependent slope. In this way we will initialise our sample of model galaxies at  $z = z_{\text{match}}$ . Making use of some parameterisations of the star formation histories for satellite and central galaxies (such as those suggested by Wang et al. 2007 or by Yang et al. 2012), we will use our model to understand when star formation has to be stopped and for which galaxies, forcing the model itself to match the SMF at low-redshift. We will then split the sample of galaxies in star-forming and passive according to some cuts in colour, with the purpose

to match the observed SMFs and the galaxy two-point correlation functions of both types of galaxies.

## ACKNOWLEDGEMENTS

EC acknowledges financial support by Chinese Academy of Sciences Presidents' International Fellowship Initiative, Grant No.2015PM054. EC, XK and AR acknowledge financial support by 973 program (No. 2015CB857003, 2013CB834900), NSF of Jiangsu Province (No. BK20140050), the NSFC (No. 11333008), and the Strategic Priority Research Program the emergence of cosmological structures of the CAS (No. XDB09010403).

## APPENDIX A: SATELLITE ABUNDANCE IN GROUPS AND CLUSTERS

In Figure A1 we plot the Conditional SMF of satellite galaxies residing in haloes of different mass, from  $\log M_{Vir}[M_\odot/h] \sim 12.9$  to  $\log M_{Vir}[M_\odot/h] \sim 14.7$ , as predicted by Model D (stars), and Model D with stripping switched off (diamonds), and compare our results with observations from SDSS survey (solid and dashed lines) by Yang et al. (2009). A model with stellar stripping and a stripping efficiency (see Section 2.2) halo mass dependent agrees better with observed data. From this figure it is also clear that a model with no stellar stripping would definitely over-predict the number density of satellites in groups over all the stellar mass range, and the number density of intermediate/massive satellites ( $\log M_*[M_\odot h^{-2}] > 10$ ) in clusters.

## REFERENCES

- Behroozi P. S., Conroy C., Wechsler R. H., 2010, *ApJ*, 717, 379
- Bernardi M., Meert A., Sheth R. K., Vikram V., Huertas-Company M., Mei S., Shankar F., 2013, *MNRAS*, 436, 697
- Brinchmann J., Charlot S., White S. D. M., Tremonti C., Kauffmann G., Heckman T., Brinkmann J., 2004, *MNRAS*, 351, 1151
- Capak P., Aussel H., Ajiki M., McCracken H. J., Mobasher B., Scoville N., Shopbell P. e. a., 2007, *ApJS*, 172, 99
- Chabrier G., 2003, *PAPS*, 115, 763
- Chaves-Montero J., Angulo R. E., Schaye J., Schaller M., Crain R. A., Furlong M., 2015, *ArXiv e-prints*
- Conroy C., Wechsler R. H., 2009, *ApJ*, 696, 620
- Conroy C., Wechsler R. H., Kravtsov A. V., 2006, *ApJ*, 647, 201
- Contini E., De Lucia G., Villalobos Á., Borgani S., 2014, *MNRAS*, 437, 3787
- Daddi E., Dickinson M., Morrison G., Chary R., Cimatti A., Elbaz D., Frayer D. e. a., 2007, *ApJ*, 670, 156
- Drory N., Bundy K., Leauthaud A., Scoville N., Capak P., Ilbert O., Kartaltepe J. S., Kneib J. P., McCracken H. J., Salvato M., Sanders D. B., Thompson D., Willott C. J., 2009, *ApJ*, 707, 1595
- D'Souza R., Vegetti S., Kauffmann G., 2015, *MNRAS*, 454, 4027
- Elbaz D., Daddi E., Le Borgne D., Dickinson M., Alexander D. M., Chary R.-R., Starck J.-L., Brandt W. N., Kitzbichler M., MacDonald E., Nonino M., Popesso P., Stern D., Vanzella E., 2007, *A&A*, 468, 33
- Fontana A., Salimbeni S., Grazian A., Giallongo E., Pentericci L., Nonino M., Fontanot F., Menci N., Monaco P., Cristiani S., Vanzella E., de Santis C., Gallozzi S., 2006, *A&A*, 459, 745
- Giacconi R., Zirm A., Wang J., Rosati P., Nonino M., Tozzi P., Gilli R., Mainieri V., Hasinger G., Kewley L., Bergeron J., Borgani S., Gilmozzi R., Grogin N., Koekemoer A., Schreier E., Zheng W., Norman C., 2002, *ApJS*, 139, 369
- Grogin N. A., Kocevski D. D., Faber S. M., Ferguson H. C., Koekemoer A. M., Riess A. G., Acquaviva V. e. a., 2011, *ApJS*, 197, 35
- Guo Q., White S., 2014, *MNRAS*, 437, 3228
- Guo Q., White S., Li C., Boylan-Kolchin M., 2010, *MNRAS*, 404, 1111
- Hearin A. P., Zentner A. R., Berlind A. A., Newman J. A., 2013, *MNRAS*, 433, 659
- Ilbert O., McCracken H. J., Le Fèvre O., Capak P., Dunlop J., Karim A., Renzini M. A. e. a., 2013, *A&A*, 556, A55
- Kang X., Jing Y. P., Mo H. J., Börner G., 2005, *ApJ*, 631, 21
- Kang X., Li M., Lin W. P., Elahi P. J., 2012, *MNRAS*, 422, 804
- Karim A., Schinnerer E., Martínez-Sansigre A., Sargent M. T., van der Wel A., Rix H.-W., Ilbert O. e. a., 2011, *ApJ*, 730, 61
- Koekemoer A. M., Faber S. M., Ferguson H. C., Grogin N. A., Kocevski D. D., Koo D. C., Lai K. e. a., 2011, *ApJS*, 197, 36
- Komatsu E., Smith K. M., Dunkley J., Bennett C. L., Gold B., Hinshaw 2011, *ApJS*, 192, 18
- Lawrence A., Warren S. J., Almaini O., Edge A. C., Hambly N. C., Jameson R. F., Lucas P. e. a., 2007, *MNRAS*, 379, 1599
- Lee N., Sanders D. B., Casey C. M., Toft S., Scoville N. Z., Hung C.-L., Le Floc'h E., Ilbert O. e. a., 2015, *ApJ*, 801, 80
- Leja J., van Dokkum P. G., Franx M., Whitaker K. E., 2015, *ApJ*, 798, 115
- Li C., White S. D. M., 2009, *MNRAS*, 398, 2177
- Longhetti M., Saracco P., 2009, *MNRAS*, 394, 774
- Lotz J. M., Jonsson P., Cox T. J., Croton D., Primack J. R., Somerville R. S., Stewart K., 2011, *ApJ*, 742, 103
- Marchesini D., van Dokkum P. G., Förster Schreiber N. M., Franx M., Labbé I., Wuyts S., 2009, *ApJ*, 701, 1765
- Moster B. P., Somerville R. S., Maubetsch C., van den Bosch F. C., Macciò A. V., Naab T., Oser L., 2010, *ApJ*, 710, 903
- Moustakas J., Coil A. L., Aird J., Blanton M. R., Cool R. J., Eisenstein D. J., Mendez A. J., Wong K. C., Zhu G., Arnouts S., 2013, *ApJ*, 767, 50
- Murante G., Giovalli M., Gerhard O., Arnaboldi M., Borgani S., Dolag K., 2007, *MNRAS*, 377, 2
- Muzzin A., Marchesini D., Stefanon M., Franx M., McCracken H. J., Milvang-Jensen B., Dunlop J. S., Fynbo J. P. U., Brammer G., Labbé I., van Dokkum P. G., 2013, *ApJ*, 777, 18
- Noeske K. G., Weiner B. J., Faber S. M., Papovich C., Koo D. C., Somerville R. S., Bundy K. e. a., 2007, *ApJ*, 660,

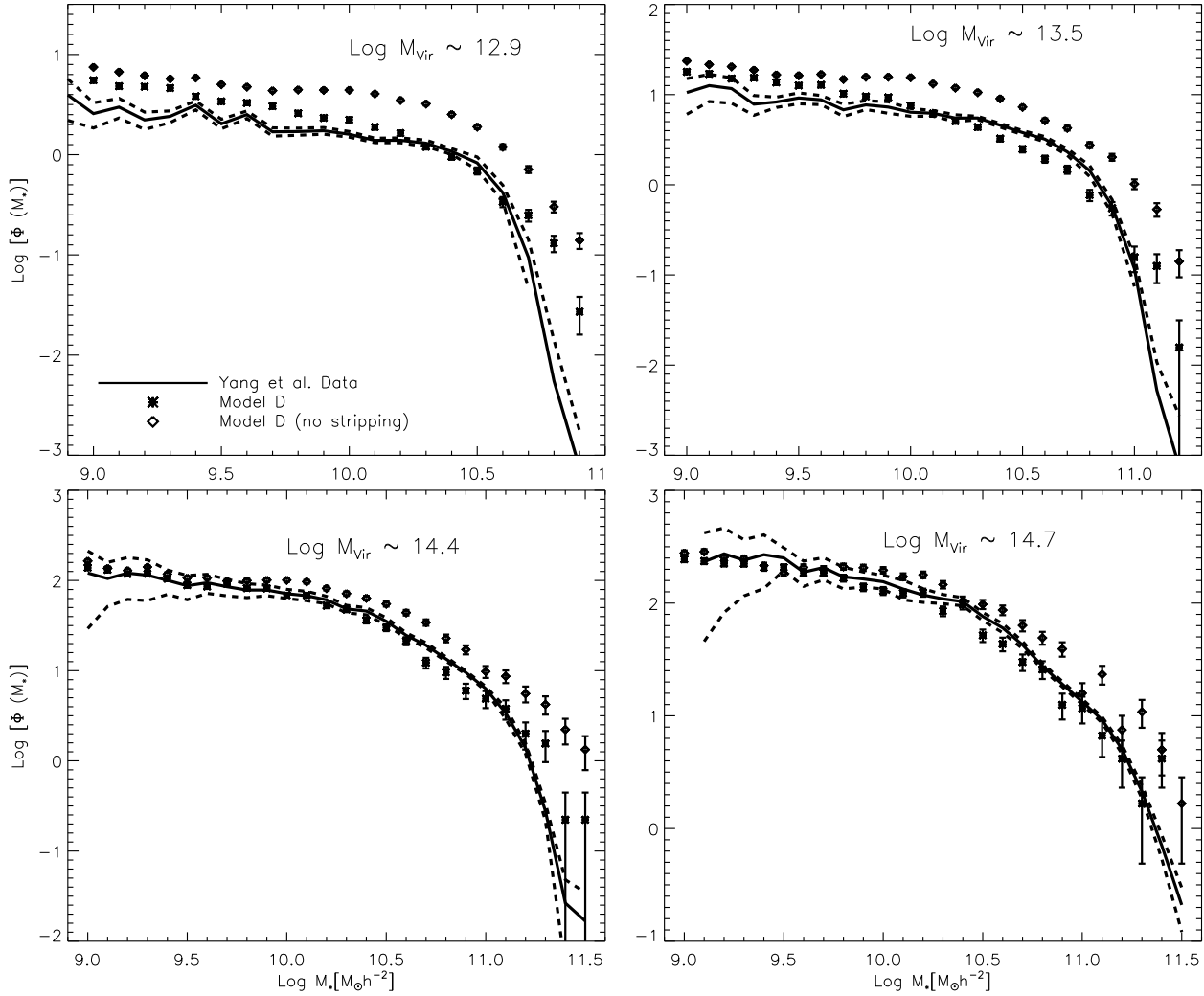


**Figure A1.** Conditional SMF (CSMF) for satellites belonging to haloes of different mass (from  $\log M_{\text{vir}} \sim 12.9$  to  $\log M_{\text{vir}} \sim 14.7$ ), as predicted by Model D (stars), Model D with no stripping (diamonds), and compared with the observed abundance from SDSS data by Yang et al. (2009). The solid lines represent the observed data while dashed lines represent the scatter.

L43  
 Peng Y. J. e. a., 2010, *ApJ*, 721, 193  
 Pérez-González P. G., Rieke G. H., Villar V., Barro G., Blaylock M., Egami E., Gallego J., Gil de Paz A., Pascual S., Zamorano J., Donley J. L., 2008, *ApJ*, 675, 234  
 Purcell C. W., Bullock J. S., Zentner A. R., 2007, *ApJ*, 666, 20  
 Renzini A., 2009, *MNRAS*, 398, L58  
 Rodighiero G., Daddi E., Baronchelli I., Cimatti A., Renzini A., Aussel H., Popesso P. e. a., 2011, *ApJ*, 739, L40  
 Salmi F., Daddi E., Elbaz D., Sargent M. T., Dickinson M., Renzini A., Bethermin M., Le Borgne D., 2012, *ApJ*, 754, L14  
 Salpeter E. E., 1955, *ApJ*, 121, 161  
 Santini P., Fontana A., Grazian A., Salimbeni S., Fontanot F., Paris D., Boutsia K., Castellano M., Fiore F., Gallozzi S., Giallongo E., Koekemoer A. M., Menci N., Pentericci L., Somerville R. S., 2012, *A&A*, 538, A33  
 Schechter P., 1976, *ApJ*, 203, 297  
 Shivaeei I., Reddy N. A., Shapley A. E., Kriek M., Siana

B., Mobasher B., Coil A. L., Freeman W. R., Sanders R., Price S. H., de Groot L., Azadi M., 2015, *ApJ*, 815, 98  
 Springel V., 2005, *MNRAS*, 364, 1105  
 Springel V., Yoshida N., White S. D. M., 2001, *NewA*, 6, 79  
 Tasca L. A. M., Le Fèvre O., Hathi N. P., Schaerer D., Ilbert O., Zamorani G., Lemaux B. C. e. a., 2015, *A&A*, 581, A54  
 Tomczak A. R., Quadri R. F., Tran K.-V. H., Labbé I., Straatman C. M. S., Papovich C., Glazebrook K. e. a., 2016, *ApJ*, 817, 118  
 Tomczak A. R., Quadri R. F., Tran K.-V. H., Labbé I. e. a., 2014, *ApJ*, 783, 85  
 Vale A., Ostriker J. P., 2004, *MNRAS*, 353, 189  
 Vale A., Ostriker J. P., 2006, *MNRAS*, 371, 1173  
 Wang L., Li C., Kauffmann G., De Lucia G., 2007, *MNRAS*, 377, 1419  
 Weinmann S. M., Pasquali A., Oppenheimer B. D., Finlator K., Mendel J. T., Crain R. A., Macciò A. V., 2012, *MNRAS*, 426, 2797

- Whitaker K. E., Franx M., Leja J., van Dokkum P. G., Henry A., Skelton R. E., Fumagalli M., Momcheva I. G., Brammer G. B., Labbé I., Nelson E. J., Rigby J. R., 2014, *ApJ*, 795, 104
- Whitaker K. E., Labbé I., van Dokkum P. G., Brammer G., Kriek M., Marchesini D., Quadri R. F. e. a., 2011, *ApJ*, 735, 86
- Whitaker K. E., van Dokkum P. G., Brammer G., Franx M., 2012, *ApJ*, 754, L29
- Williams R. J., Quadri R. F., Franx M., 2011, *ApJ*, 738, L25
- Yamamoto M., Masaki S., Hikage C., 2015, *ArXiv e-prints*
- Yang X., Mo H. J., van den Bosch F. C., 2009, *ApJ*, 695, 900
- Yang X., Mo H. J., van den Bosch F. C., Zhang Y., Han J., 2012, *ApJ*, 752, 41